Displacement of a two-dimensional immiscible droplet in a channel

Qinjun Kang
Los Alamos National Laboratory, Los Alamos, New Mexico 87545
and The Johns Hopkins University, Baltimore, Maryland 21218

Dongxiao Zhang
Los Alamos National Laboratory, Los Alamos, New Mexico 87545

Shiyi Chen
The Johns Hopkins University, Baltimore, Maryland 21218
and Peking University, Beijing, China

We used the lattice Boltzmann method to study the displacement of a two-dimensional immiscible droplet subject to gravitational forces in a channel. The dynamic behavior of the droplet is shown, and the effects of the contact angle, Bond number (the ratio of gravitational to surface forces), droplet size, and density and viscosity ratios of the droplet to the displacing fluid are investigated. For the case of a contact angle less than or equal to 90°, at a very small Bond number, the wet length between the droplet and the wall decreases with time until a steady shape is reached. When the Bond number is large enough, the droplet first spreads and then shrinks along the wall before it reaches steady state. Whether the steady-state value of the wet length is greater or less than the static value depends on the Bond number. When the Bond number exceeds a critical value, a small portion of the droplet pinches off from the rest of the droplet for a contact angle less than 90°; a larger portion of the droplet is entrained into the bulk for a contact angle equal to 90°. For the nonwetting case, however, for any Bond number less than a critical value, the droplet shrinks along the wall from its static state until reaching the steady state. For any Bond number above the critical value, the droplet completely detaches from the wall. Either increasing the contact angle or viscosity ratio or decreasing the density ratio decreases the critical Bond number. Increasing the droplet size increases the critical Bond number while it decreases the critical capillary number. © *2002 American Institute of Physics.* [DOI: 10.1063/1.1499125]

I. INTRODUCTION

Multiphase or multicomponent flow in porous media is an important phenomenon for a wide range of practical problems, including oil recovery and the transport of nonaqueous-phase liquid contamination in the soil via water or surfactant flooding. The study of the displacement of immiscible fluids in a single pore throat is a prerequisite for simulating flow in porous materials, which consist of networks of pore throats and pore bodies. Previous work on immiscible displacement in capillary tubes has focused on the displacement of a fluid meniscus,[1] the displacement of freely suspended fluid droplets,[2–4] and the displacement of a droplet attached to the wall where the no-slip boundary condition is enforced and the contact lines remain pinned to their initial positions.[5–9]

Most immiscible displacement-related problems in capillary tubes are a moving contact-line problem, which is important both from a purely theoretical and a practical point of view, and has attracted the attention of many investigators.[1,10–15] A direct application of classical hydrodynamics on the liquid/liquid/solid systems encounters fundamental difficulties. Assumptions need to be made to describe the behavior of the dynamic contact angle and to remove the nonintegrable stress singularity at the dynamic contact lines.[15]

To overcome these problems, Shikhmurzaev developed a general mathematical model that describes, in the case of small capillary number and small Reynolds number, the motion of an interface between immiscible viscous fluids along a smooth homogeneous solid surface.[15] Molecular dynamics simulations are also used to study the immiscible fluid system.[14] Koplik's simulations confirm Dussan's theoretical predictions of the breakdown of the no-slip condition.[10] The lattice Boltzmann (LB) method, a promising numerical method, is also applied to the moving contact-line problem.[16–18] Although different methods have been applied to study a variety of immiscible fluid systems, the displacement of an immiscible droplet adhering to a wall in a channel under external forces has received less attention. This problem is particularly interesting and challenging because there is a coalescence of contact lines when the droplet detaches from the wall.

Using a boundary-integral method, Schleizer and Bonnecaze[19] studied the dynamic behavior and stability of a two-dimensional immiscible droplet subject to shear or pressure-driven flow under conditions where inertial and gravitational forces can be neglected. The droplet is attached to the solid surface, and the two contact lines are either fixed or mobile. To allow the droplet to slip along the wall, they applied an integral form of the Navier-slip model while

3203

keeping the contact angle fixed. They investigated the effects of contact angle, capillary number (the ratio of viscous to surface forces), droplet size, and viscosity ratio on the droplet behavior. Their simulation results showed that for contact angles less than or equal to 90°, a stable droplet spreads along the wall until a steady shape is reached; the droplet then moves across the wall at a constant velocity.

For contact angles greater than 90°, the wet length between a stable droplet and the wall decreases until a steady shape is reached. They also claimed that above a critical capillary number, the droplet completely detaches for a contact angle of 120°. However, they indicated that it was too difficult to include the coalescence of the contact lines in their numerical method. In this respect, the LB method may be an alternative numerical approach that is capable of naturally simulating the coalescence of contact lines.[20,21]

Unlike conventional numerical schemes based on discretizations of macroscopic continuum equations, the LB method is based on microscopic models and mesoscopic kinetic equations,[22] giving the LB method the advantage in the study of nonequilibrium dynamics, especially in fluid-flow applications involving interfacial dynamics and complex boundaries (geometries). The LB method has also proved to be competitive in studying a variety of flow and transport phenomena (see Refs. 22–26 for reviews), including flow or chemical dissolution in porous media.[27,28] One particular application of the LB method that has attracted considerable attention is modeling the flows of multiphase or multicomponent fluids. These flows are important, but because of the complex interfaces in the inhomogeneous flows, they are difficult to simulate with the conventional technique of solving Navier–Stokes-type macroscopic equations. The LB method, however, because of its kinetic nature, can handle these problems more easily.[22] Although the LB method cannot simulate the moving contact-line problem on the microscopic scale as molecular dynamics does, it can simulate physics on a scale smaller than the macroscopic methods based on the Navier–Stokes-type equations and can simulate mesoscopic-level physics, which may be important in this problem. In simulating the immiscible displacement of a droplet with the LB method, no assumption about the relationship between the contact angle and velocity of the contact line is necessary, and the coalescence of the contact lines can be demonstrated naturally.

There are four LB models used for the study of multiphase and/or multicomponent flow. The first model, using a recoloring process,[29,30] is quite robust and its algorithm is straightforward. However, it has two drawbacks: first, the recoloring process requires time-consuming calculations for the local maxima; second, the perturbation step with the redistribution of colored distribution functions causes an anisotropic surface tension that induces unphysical vortices near interfaces.[22] The second model makes use of an interparticle potential.[31–34] This model has a correct physical basis and gives a nonideal equation of state. The isotropy of the surface tension at the interface is improved.[35] The separation of a two-phase fluid into its components is automatic.[22] The third model, with free energy,[36,37] is the first LB two-phase thermal model, and it also has a sound physical basis. It

produces a correct equation of state and has a consistent surface tension representation. However, it does not satisfy Galilean invariance. Its macroscopic equation has a velocity-dependent pressure.[38] The fourth model can be considered to be a significant modification of the second model.[39] In addition to the attractive force, a repulsive force is included. The numerical stability is improved by reducing the effect of numerical errors in the calculation of molecular interactions. An index function is used to track the interfaces between different phases. All of the above models have been successfully used in various applications, including flow through porous media[40–43] and Rayleigh–Taylor instability.[39,44]

In this paper, we use the model with interparticle potential. Besides the above-mentioned reasons, this model is convenient for implementing different wettabilities and handling fluids with different densities and viscosities. With this model, we have studied the dynamic behavior of a two-dimensional immiscible droplet in a simple channel subject to gravitational forces and assessed the effects of the contact angle, Bond number, droplet size, and the density and viscosity ratios of the droplet to the displacing fluid.

II. MODEL AND THEORY

A. Multiphase or multicomponent lattice Boltzmann model

Let us first review the multiphase or multicomponent LB model proposed by Shan and Chen.[31,32] Their model allows for density distribution functions of an arbitrary number of components with different molecular mass. The interaction between the particles is included in the kinetics through a set of potentials. The LB equations for the kth component can be written in the following form:

$$f_i^k(\mathbf{x}+\mathbf{e}_i\delta_t,t+\delta_t)-f_i^k(\mathbf{x},t)=-\frac{f_i^k(\mathbf{x},t)-f_i^{k(\mathrm{eq})}(\mathbf{x},t)}{\tau_k}, \quad (1)$$

where $f_i^k(\mathbf{x},t)$ is the number density distribution in the ith velocity direction for the kth fluid at position $\mathbf{x}$ and time t, and δ_t is the time increment. On the right-hand side, τ_k is the relaxation time of the kth component and is in the lattice unit, and $f_i^{k(\mathrm{eq})}(\mathbf{x},t)$ is the corresponding equilibrium distribution function. For a two-dimensional 9-speed LB model (D2Q9, where D is the dimension and Q is the number of velocity directions), $f_i^{k(\mathrm{eq})}(\mathbf{x},t)$ has the following form:[45,46]

$$f_0^{f(\mathrm{eq})}=\alpha_k n_k-\frac{2}{3}n_k\mathbf{u}_k^{\mathrm{eq}}\cdot\mathbf{u}_k^{\mathrm{eq}},$$

$$f_i^{k(\mathrm{eq})}=\frac{(1-\alpha_k)n_k}{5}+\frac{1}{3}n_k(\mathbf{e}_i\cdot\mathbf{u}_k^{\mathrm{eq}})$$

$$+\frac{1}{2}n_k(\mathbf{e}_i\cdot\mathbf{u}_k^{\mathrm{eq}})^2-\frac{1}{6}n_k\mathbf{u}_k^{\mathrm{eq}}\cdot\mathbf{u}_k^{\mathrm{eq}} \quad \text{for } i=1,...,4, \quad (2)$$

$$f_i^{k(\text{eq})} = \frac{(1-\alpha_k)n_k}{20} + \frac{1}{12} n_k(\mathbf{e}_i \cdot \mathbf{u}_k^{\text{eq}})$$

$$+ \frac{1}{8} n_k(\mathbf{e}_i \cdot \mathbf{u}_k^{\text{eq}})^2 - \frac{1}{24} n_k \mathbf{u}_k^{\text{eq}} \cdot \mathbf{u}_k^{\text{eq}} \quad \text{for } i=5,...,8.$$

In the above equations, $\mathbf{e}_i$'s are the discrete velocities, which are chosen to be

$$\mathbf{e}_i = \begin{cases} \mathbf{0}, & i=0, \\ \left(\cos\frac{(i-1)\pi}{2}, \sin\frac{(i-1)\pi}{2} \right), & i=1-4, \\ \sqrt{2}\left(\cos\left[\frac{(i-5)\pi}{2}+\frac{\pi}{4}\right], \sin\left[\frac{(i-5)\pi}{2}+\frac{\pi}{4}\right] \right), & i=5-8, \end{cases} \tag{3}$$

α_k is a free parameter, which relates to the sound speed of a region of pure kth component as $(c_s^k)^2 = \frac{3}{5}(1-\alpha_k)$;[46] $n_k = \Sigma_i f_i^k$ is the number density of the kth component. The mass density of the kth component ρ_k is defined as $\rho_k = m_k n_k = m_k \Sigma_i f_i^k$, and the fluid velocity of the kth fluid $\mathbf{u}_k$ is defined through $\rho_k \mathbf{u}_k = m_k \Sigma_i \mathbf{e}_i f_i^k$, where m_k is the molecular mass of the kth component. The parameter $\mathbf{u}_k^{\text{eq}}$ is determined by the relation

$$\rho_k \mathbf{u}_k^{\text{eq}} = \rho_k \mathbf{u}' + \tau_k \mathbf{F}_k, \tag{4}$$

where $\mathbf{u}'$ is a common velocity on top of which an extra component-specific velocity due to interparticle interaction is added for each component, and $\mathbf{F}_k = \mathbf{F}_{1k} + \mathbf{F}_{2k} + \mathbf{F}_{3k}$ is the total force acting on the kth component, including fluid–fluid interaction $\mathbf{F}_{1k}$, fluid–solid interaction $\mathbf{F}_{2k}$, and external force $\mathbf{F}_{3k}$.[42] To conserve momentum at each collision in the absence of interaction (i.e., in the case of $\mathbf{F}_k = 0$), $\mathbf{u}'$ has to satisfy the relation

$$\mathbf{u}' = \left(\sum_{k=1}^{s} \frac{\rho_k \mathbf{u}_k}{\tau_k} \right) \bigg/ \left(\sum_{k=1}^{s} \frac{\rho_k}{\tau_k} \right). \tag{5}$$

The interactive force between particles of the kth component at site $\mathbf{x}$ and the $\bar{k}$th component at site $\mathbf{x}'$ is assumed to be proportional to the product of their "effective number density" $\psi_k(n_k)$ defined as a function of local number density. The total fluid–fluid interactive force on the kth component at site $\mathbf{x}$ is

$$\mathbf{F}_{1k}(\mathbf{x}) = -\psi_k(\mathbf{x}) \sum_{\mathbf{x}'} \sum_{\bar{k}=1}^{s} G_{k\bar{k}}(\mathbf{x},\mathbf{x}') \psi_{\bar{k}}(\mathbf{x}')(\mathbf{x}'-\mathbf{x}), \tag{6}$$

where $G_{k\bar{k}}(\mathbf{x},\mathbf{x}')$ satisfies $G_{k\bar{k}}(\mathbf{x},\mathbf{x}') = G_{k\bar{k}}(\mathbf{x}',\mathbf{x})$, and $\psi_k(\mathbf{x})$ is a function of $\mathbf{x}$ through its dependency of n_k. The above form of interaction potential was originally used for single-speed lattices such as the two-dimensional hexagonal and the four-dimensional FCHC,[31] and only homogeneous isotropic interactions between the nearest neighbors were considered. The interaction potential of the D2Q9 lattice can be obtained with a similar method adopted by Martys and Chen[42] to project the interaction potential from 4D FCHC lattice to the D3Q19 model. In this case, the nearest-neighbor interaction

in four dimensions corresponds to a potential that couples nearest and next-nearest neighbors in the D2Q9 lattice model. In this case,

$$G_{k\bar{k}}(\mathbf{x},\mathbf{x}') = \begin{cases} g_{k\bar{k}}, & |\mathbf{x}-\mathbf{x}'|=1, \\ g_{k\bar{k}}/4, & |\mathbf{x}-\mathbf{x}'|=\sqrt{2}, \\ 0, & \text{otherwise}. \end{cases} \tag{7}$$

Here $g_{k\bar{k}}$ is the strength of the interparticle potential between component k and $\bar{k}$. The effective number density $\psi_k(n_k)$ is taken as n_k in this study. Other choices will give a different equation of state.

At the fluid/solid interface, the wall is regarded as a phase with a constant number density. The interactive force between the fluid and wall is described as

$$\mathbf{F}_{2k}(\mathbf{x}) = -n_k(\mathbf{x}) \sum_{\mathbf{x}'} g_{kw} n_w(\mathbf{x}')(\mathbf{x}'-\mathbf{x}), \tag{8}$$

where n_w is the number density of the wall, which is a constant at the wall and zero elsewhere, and g_{kw} is the interactive strength between component k and the wall. g_{kw} is positive for a nonwetting fluid and negative for a wetting fluid. By adjusting it, we can get different wettabilities.

The action of a constant body force can be simply introduced as

$$\mathbf{F}_{3k} = \rho_k \mathbf{g} = m_k n_k \mathbf{g}, \tag{9}$$

where $\mathbf{g}$ is the body force per unit mass.

The Chapman–Enskog expansion procedure can be carried out to obtain the following continuity and momentum equations for the fluid mixture as a single fluid:[33]

$$\frac{\partial \rho}{\partial t} + \nabla \cdot (\rho \mathbf{u}) = 0, \tag{10}$$

$$\rho \left[\frac{\partial \mathbf{u}}{\partial t} + (\mathbf{u} \cdot \nabla)\mathbf{u} \right] = -\nabla p + \nabla \cdot [\rho \nu(\nabla \mathbf{u} + \mathbf{u}\nabla)] + \rho \mathbf{g}, \tag{11}$$

where $\rho = \Sigma_k \rho_k$ is the total density of the fluid mixture, and the whole fluid velocity $\mathbf{u}$ is defined by $\rho \mathbf{u} = \Sigma_k \rho_k \mathbf{u}_k + \frac{1}{2}\Sigma_k \mathbf{F}_k$.[34] Notice that the introduction of fluid–solid interaction has no effect on the macroscopic equations since $\mathbf{F}_{2k}$ only exists at the solid/fluid interface.

Since the Shan–Chen model was proposed, it has been widely used by various investigators. Hou et al.[35] performed a static bubble test with this model. Their results show that a physically correct isotropic, stable bubble satisfying Laplace's law can be simulated. Fan et al.[16] applied the model to the simulation of contact line dynamics in a two-dimensional capillary tube. In their paper, the velocity dependency of the contact angle is studied for two different wetting cases. Their simulation results are in good agreement with those based on theoretical computations and with molecular dynamics simulations. Martys and Chen[42] used this model to simulate the multicomponent fluid flow in complex three-dimensional geometries. In their study, the displacement of one fluid by another in a porous medium was modeled. The relative permeability for different wetting fluid saturations of a microtomography-generated image of sandstone was calculated and compared favorably with experi-

ment. Sehgal *et al.*[47] developed a FlowLab code based on this model and performed a series of multiphase flow benchmark tests, including a static bubble test, a phase transition test, and the test of agglomeration of two immiscible fluids. They then applied this method to the simulation of droplet deformation and breakup. The deformation/breakup regime map, derived from their simulation results, is in quite good agreement with experimental data. All the numerical simulations show that the hydrodynamics from this method are correct.

B. Application to systems of immiscible fluids with different densities and viscosities

The previous applications of the above LB model to systems of immiscible fluids considered only fluids with the same molecular mass and viscosity.[16,35,42,47] Our study, however, aims to study the effects of density and viscosity ratios between the displaced and displacing fluids.

When the above equilibrium distribution function, Eq. (2), is chosen, in a region of pure kth component, the pressure is given by $p_k = (c_s^k)^2 \rho_k = (c_s^k)^2 m_k n_k$, where $(c_s^k)^2 = \frac{3}{5}(1 - \alpha_k)$. To simulate a multiple component fluid with different component densities, we let $(c_s^k)^2 m_k = c_0^2$, where c_0^2 is a constant. In this study, $c_0^2 = \frac{1}{3}$, and $m_k \geq 1$. Then the pressure of the whole fluid is given by $p = c_0^2 \Sigma_k n_k + \frac{3}{2} \Sigma_{k,\bar{k}} g_{k,\bar{k}} \psi_k \psi_{\bar{k}}$, which represents a nonideal gas law. The viscosity is given by $\nu = \frac{1}{3}(\Sigma_k \beta_k \tau_k - \frac{1}{2})$, where β_k is the mass density concentration of the kth component and is defined as $\rho_k / \Sigma_k \rho_k$.[35]

III. SIMULATION RESULTS AND DISCUSSION

The two-dimensional geometry used in our simulations is shown in Fig. 1, where an immiscible droplet (fluid 2) with area A is put into a two-dimensional channel filled with fluid 1. The letters l and h are the length and width of the channel, respectively; b_0 is the wet length between the droplet and the wall; a_0 is the droplet height; and θ_1 and θ_2 are the contact angles of fluid 1 and 2, respectively. The contact angle is defined as the angle between a two-fluid interface and a solid surface. As shown in Fig. 1, each fluid has its own contact angle and the sum of the two must equal 180°. The wetting fluid (the fluid that tends to wet the surface) has a contact angle of less than 90°, and the nonwetting fluid (the fluid that has less affinity for the solid surface) has a contact angle of greater than 90°.

From simple geometry, R, the radius of the droplet, can be calculated[48] from the final steady values of a_0 and b_0 as

$$R = \frac{a_0}{2} + \frac{b_0^2}{8a_0}. \tag{12}$$

The contact angle of the droplet satisfies the following relation:[48]

$$\tan(\theta_2) = \frac{b_0}{2(R - a_0)}. \tag{13}$$

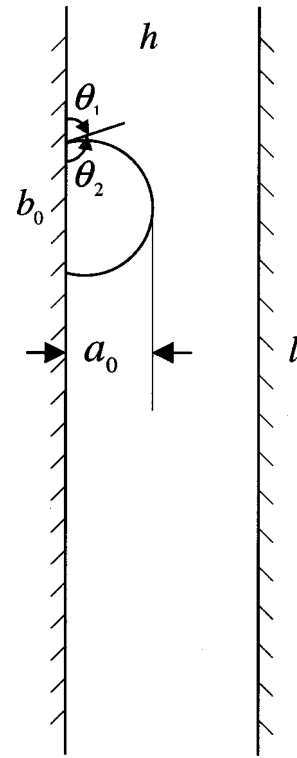The area, the radius, and the contact angle of the droplet satisfy the following equation:

FIG. 1. Schematic illustration of simulation geometry.

$$A = R^2(\theta_2 - 0.5 \sin(2\theta_2)). \tag{14}$$

For simplicity, hereafter we refer to θ_2 when we say contact angle or θ. The coordinate origin is located at the bottom left corner. A particle distribution function bounce-back scheme[49,50] is used at the walls to obtain no-slip velocity conditions. By the so-called bounce-back scheme, we mean that when a particle distribution streams to a wall node, the particle distribution scatters back to the node it came
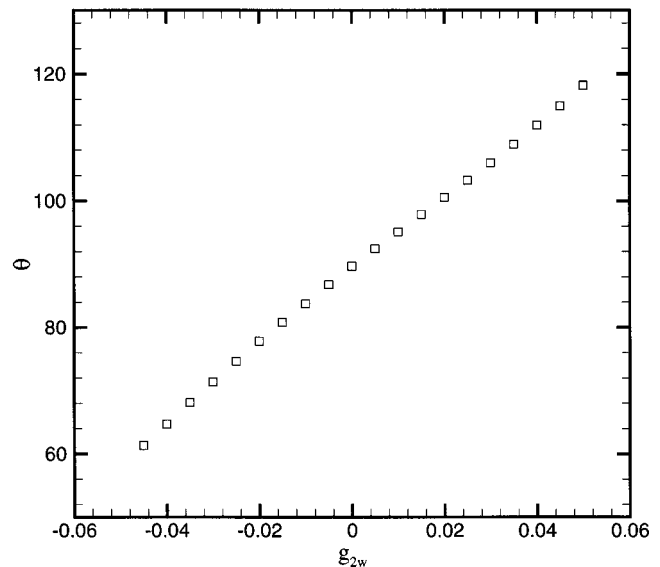

FIG. 2. The dependency of the contact angle of the droplet, θ, on the interparticle potential between the droplet and the wall, g_{2w}. Other parameters are $\rho_2/\rho_1 = 1$, $\nu_2/\nu_1 = 1$, $g_{12} = g_{21} = 0.2$, and $A/h^2 = 0.31$.
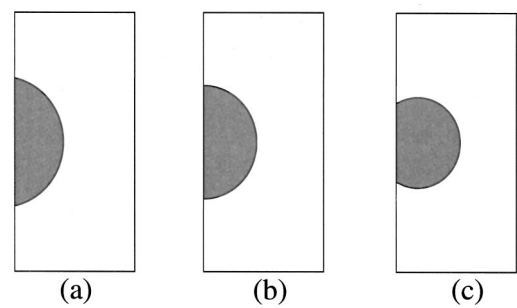
FIG. 3. Three static contact angles obtained by adjusting g_{2w}, the parameters are the same as in Fig. 2: (a) $g_{2w} = -0.02$, $\theta = 78°$, (b) $g_{2w} = 0$, $\theta = 90°$, (c) $g_{2w} = 0.05$, $\theta = 118°$.
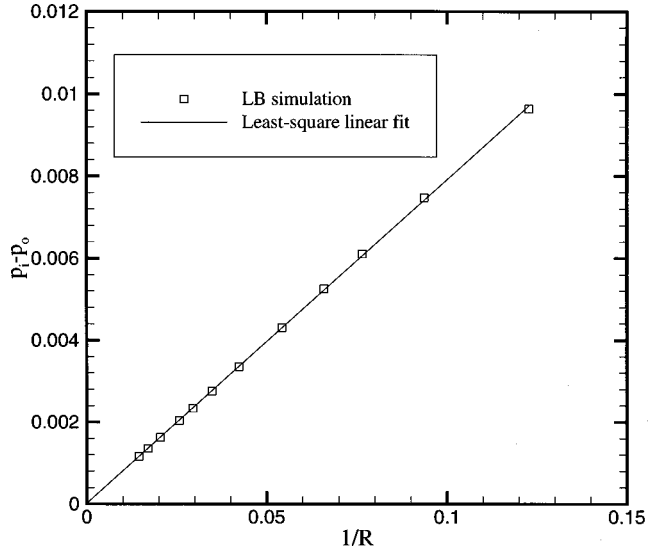

FIG. 4. Test of Laplace's law, the slope (i.e., the surface tension) is 0.078 94; the intercept is 0.000 0176; and the coefficient of determination is 0.999 85.

from. Periodic boundary conditions are applied at $y = 0$ and $y = l$. The flow is induced by a constant body force along the $-y$ direction.

A. Evaluation of contact angle

The static contact angle can be reasonably well predicted by Eq. (8).[42] In this simulation, no body force is applied, and $l = 300$, $h = 40$, both in lattice unit spacings, $A/h^2 = 0.31$, $\rho_2/\rho_1 = 1$, $\nu_2/\nu_1 = 1$, $g_{1w} = -g_{2w}$, $g_{11} = g_{22} = 0$, and $g_{12} = g_{21} = 0.2$. Initially, $b_0 = 2a_0 = 2R$. When a static droplet is obtained, the values of a_0 and b_0 are measured, and R and θ are calculated from Eqs. (12) and (13), respectively. The values of g_{1w} and g_{2w} are varied to obtain steady droplets with different contact angles. The contact angle is a linear function of g_{2w}, which is in agreement with the work of Yang et al.[51] As shown in Fig. 2, θ is less than 90° when g_{2w} is negative, which means fluid 2 tends to wet the surface; θ is equal to 90° when g_{2w} equals zero, indicating that neither of the fluids has the preference to wet the surface; and θ is greater than 90° when g_{2w} is positive, meaning that the fluid 2 is nonwetting to the wall. Hence by adjusting g_{2w}, we may obtain different contact angles, i.e., different wettabilities. As shown in Fig. 3, contact angles 78°, 90°, and 118° are obtained by letting g_{2w} equal -0.02, 0, and 0.05, respectively.

B. Evaluation of surface tension

Previous tests of Laplace's law with this LB model were performed in situations where periodic boundary conditions were applied in all directions.[31,35,42,47] In this study, however, we performed the bubble test with the existence of the wall to test the correctness of the method handling the fluid–fluid as well as the fluid–solid interactions. Laplace's law[48] states

$$p_i - p_o = \frac{\sigma}{R}, \tag{15}$$

where p_i and p_o are the pressure inside and outside the droplet, respectively; σ is the surface tension between fluid 1 and 2; and R is the radius of the droplet.

In this simulation, there is no body force applied, and $l = 300$, $h = 150$, fluid 1 and 2 have the same density and viscosity, $g_{11} = g_{22} = 0$, and $g_{12} = g_{21} = 0.2$. The values of g_{1w} and g_{2w}, as well as the initial values of a_0 and b_0, are varied to obtain steady droplets with different radii and contact angles. The final droplet radius and pressure difference between the inside and outside of the droplet are measured. Steady-state pressure inside the droplet (p_i) and outside the droplet (p_o) is measured on nodes that are away from the interface since the values of the pressure vary near the interface.[35] These results are listed in Table I and plotted in Fig. 4. The droplet radius, pressure difference, and calculated surface tension are all in lattice units and can be related to practical problems. The square symbols in Fig. 4 indicate the results of the LB simulations, and the solid line is the least-square linear fit. The slope (i.e., the surface tension) is 0.078 94; the intercept is 0.000 0176; and the coefficient of determination is 0.999 85. It is clear that all points fit a straight line through the origin quite well. The pressure difference inside and outside the bubble is indeed proportional to the reciprocal of the radius. It is clear that Laplace's law is well satisfied in the bubble test simulations with the existence of the wall. The agreement between the theory and our numerical simulation indicates that the described LB method
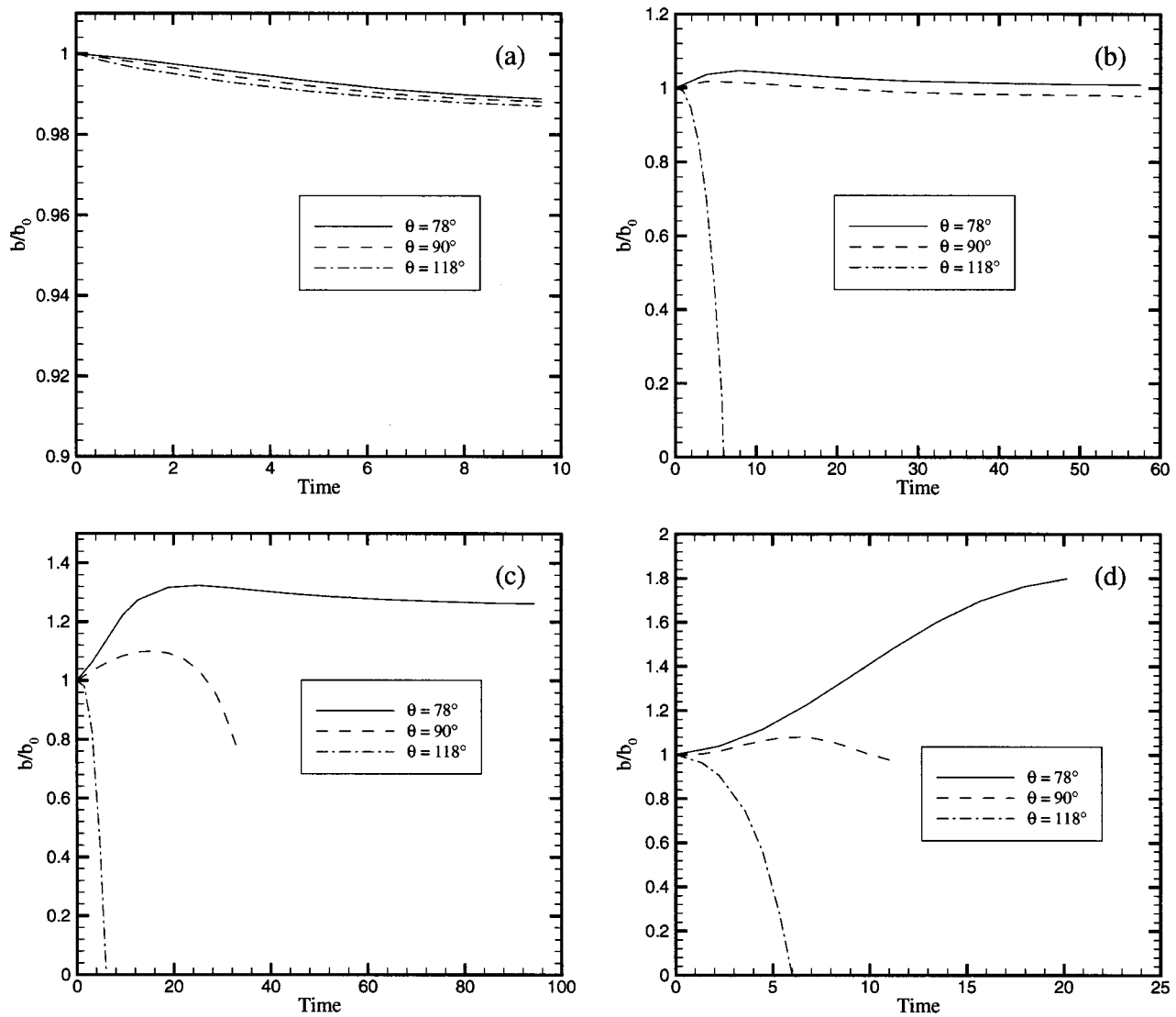
TABLE I. Test of Laplace's law.

Radius	8.145 079	10.673 730	13.060 358	15.165 089	18.432 281	23.592 344
Δp	0.009 636	0.007 469	0.006 107	0.005 249	0.004 308	0.003 355
σ	0.078 486	0.079 722	0.079 760	0.079 601	0.079 406	0.079 152
Radius	28.679 053	33.801 003	38.815 093	48.828 534	58.803 024	68.801 342
Δp	0.002 757	0.002 341	0.002 040	0.001 626	0.001 355	0.001 163
σ	0.079 068	0.079 128	0.079 183	0.079 395	0.079 678	0.080 016

FIG. 5. Evolution of the dimensionless wet length b/b_0 between the wall and the sliding droplet at three contact angles ($\theta = 78°$, 90°, and 118°), where b_0 is the wet length at time 0. Time is made dimensionless by characteristic time l/U. Other parameters are the same as in Fig. 2: (a) $B_0 = 0.061\,42$, (b) $B_0 = 0.3685$, (c) $B_0 = 0.6044$, (d) $B_0 = 0.8599$.

handles the fluid–fluid interaction and fluid–solid interaction correctly.

C. Displacement of droplet

In the following simulations, l is 300 and h is 40. After a static droplet is achieved at time zero, a constant body force (gravitational force) is applied to both the displacing fluid and the droplet along the $-y$ direction. The simulation goes on until steady state is reached or part of the droplet pinches off from the rest, or the entire droplet detaches from the wall. The steady state here is defined as the state at which the droplet moves along the wall with a constant velocity and its shape does not change with time. Numerically, the steady state is reached when the wet length between the droplet and wall varies less than 0.1% in 1000 successive time steps. The effects of the static contact angle, the Bond number, the droplet size, and the density and viscosity ratios between the two fluids are investigated. In what follows, we define U

$= \rho_1 g h^2 / \mu_1$ as the characteristic velocity, and l/U as the characteristic time, where ρ_1 and μ_1 are the density and viscosity of fluid 1, respectively. The Bond number is defined as $B_0 = \rho_2 g A / \sigma$, where ρ_2 is the density of fluid 2, and g is the gravitational factor. The Bond number is a dimensionless parameter that indicates the ratio of gravitational force to surface force.

1. Effect of contact angle

Figure 5 shows the time evolution of the dimensionless wet length b/b_0 between the wall and the sliding droplet with $\rho_2 / \rho_1 = 1$, $\nu_2 / \nu_1 = 1$, and $A/h^2 = 0.31$, at three contact angles ($\theta = 78°$, 90°, and 118°) and four Bond numbers (0.061 42, 0.3685, 0.6044, and 0.8599). Different Bond numbers are obtained by changing g, the gravitational factor. At a very low Bond number of 0.061 42 [Fig. 5(a)], b/b_0 decreases with time for all contact angles before it reaches a steady-state value, and the three curves are very close to each

other. At a moderate Bond number of 0.3685 [Fig. 5(b)], the three curves begin to separate. For both $\theta=78°$ (wetting case) and $\theta=90°$, b/b_0 increases with time at first, then decreases. The steady-state value of b/b_0 is greater than 1 in the former case and smaller than 1 in the latter case. Whether the steady-state value of b/b_0 is greater or less than 1 depends on the Bond number (see Fig. 10 for details). For the cases of $\theta=118°$ (nonwetting case), b/b_0 dramatically decreases with time and reaches 0 at time 6, when the droplet totally detaches from the wall. In this nonwetting case, the Bond number already exceeds a critical value called critical Bond number (B_0^c), below which a sliding droplet with a constant shape may be observed, and above which no steadily sliding droplet will be obtained. At a high Bond number of 0.6044, as shown in Fig. 5(c), in the wetting case, b/b_0 increases rapidly at first and then gradually decreases before it plateaus to a value of about 1.26. The nonwetting droplet again dramatically shrinks along the wall with time and detaches from the wall at time 6.

The behavior of the droplet with $\theta=90°$, however, is more complicated. It spreads along the wall at first, then shrinks. Its upper portion deforms and moves faster than the lower portion and eventually pinches off. Hence this Bond number also exceeds the critical value of the droplet in this case. The highest Bond number of 0.8599 is greater than the critical Bond number of all three cases; thus no steadily sliding droplet will be observed. However, the droplet with different static contact angles behaves very differently. When $\theta=78°$, the droplet spreads along the wall continuously before a portion of it pinches off and is entrained into the bulk flow. When $\theta=90°$, the droplet spreads along the wall at first and then shrinks, and the upper portion of the droplet pinches off when the droplet is shrinking. When $\theta=118°$, the downstream contact line moves more slowly than the upstream contact line all the way, and the contact lines eventually come together; thus the entire droplet detaches from the wall.

The dynamic process of the droplet with the three contact angles detaching from the wall at Bond number 0.8599 is shown in Fig. 6. It is clear from Fig. 6 that the detached portion of the droplet at $\theta=90°$ is larger than that at $\theta=78°$, which confirms the assertion by Schleizer and Bonnecaze[19] that above the critical capillary number, increasing the contact angle results in a larger fraction of droplet being entrained in the bulk. Figure 7 shows the corresponding velocity fields of the detaching process. We can see that when $\theta=78°$ and $90°$, the velocity inside the upper portion of the droplet is larger than that inside the lower portion, which causes the upper portion to translate more rapidly and eventually pinches off from the lower portion. When $\theta=118°$, however, the velocity inside the droplet is almost uniform and larger than that of fluid 1 near the wall. That means the shear forces between the droplet and the wall are very large and eventually cause the entire droplet to detach from the wall. Figure 8 shows the velocity fields when the droplet is steadily sliding along the wall. Note that the no-slip boundary condition is well satisfied. The velocity field relative to the average droplet velocity reveals, in Figs. 8(d)–8(f), a vortex flow pattern within the droplet itself, which is
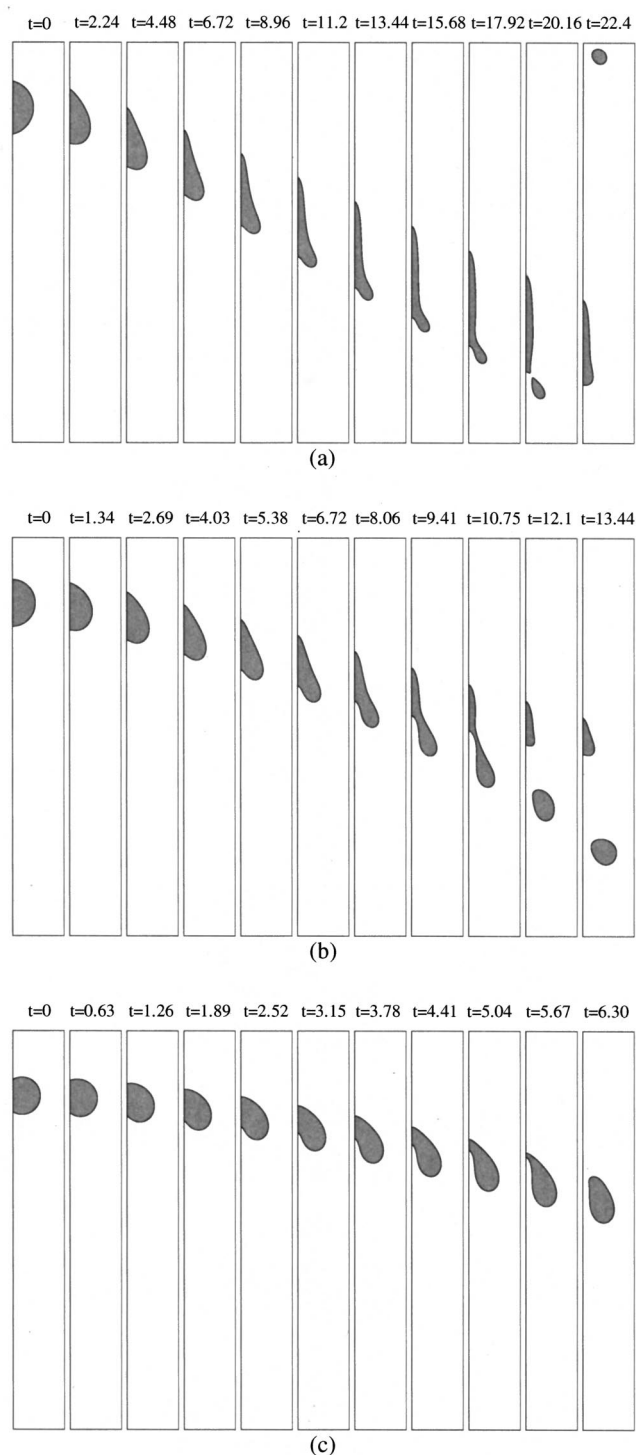

FIG. 6. Dynamic behavior of the droplet at $B_0=0.8599$, corresponding to Fig. 5(d): (a) $\theta=78°$, a small portion of the droplet pinches off from the rest. At $t=22.4$, the detached portion re-enters the system due to the periodic conditions applied along y direction, (b) $\theta=90°$, a large portion of the droplet pinches off from the rest, (c) $\theta=118°$, the entire droplet detaches from the wall.

very similar to that obtained by Grubert and Yeomans.[18]

From the above discussion, we notice that the critical Bond number of $\theta=90°$ is smaller than that of $\theta=78°$ but greater than that of $\theta=118°$. Figure 9 shows a general relationship between the critical Bond number and the static con-
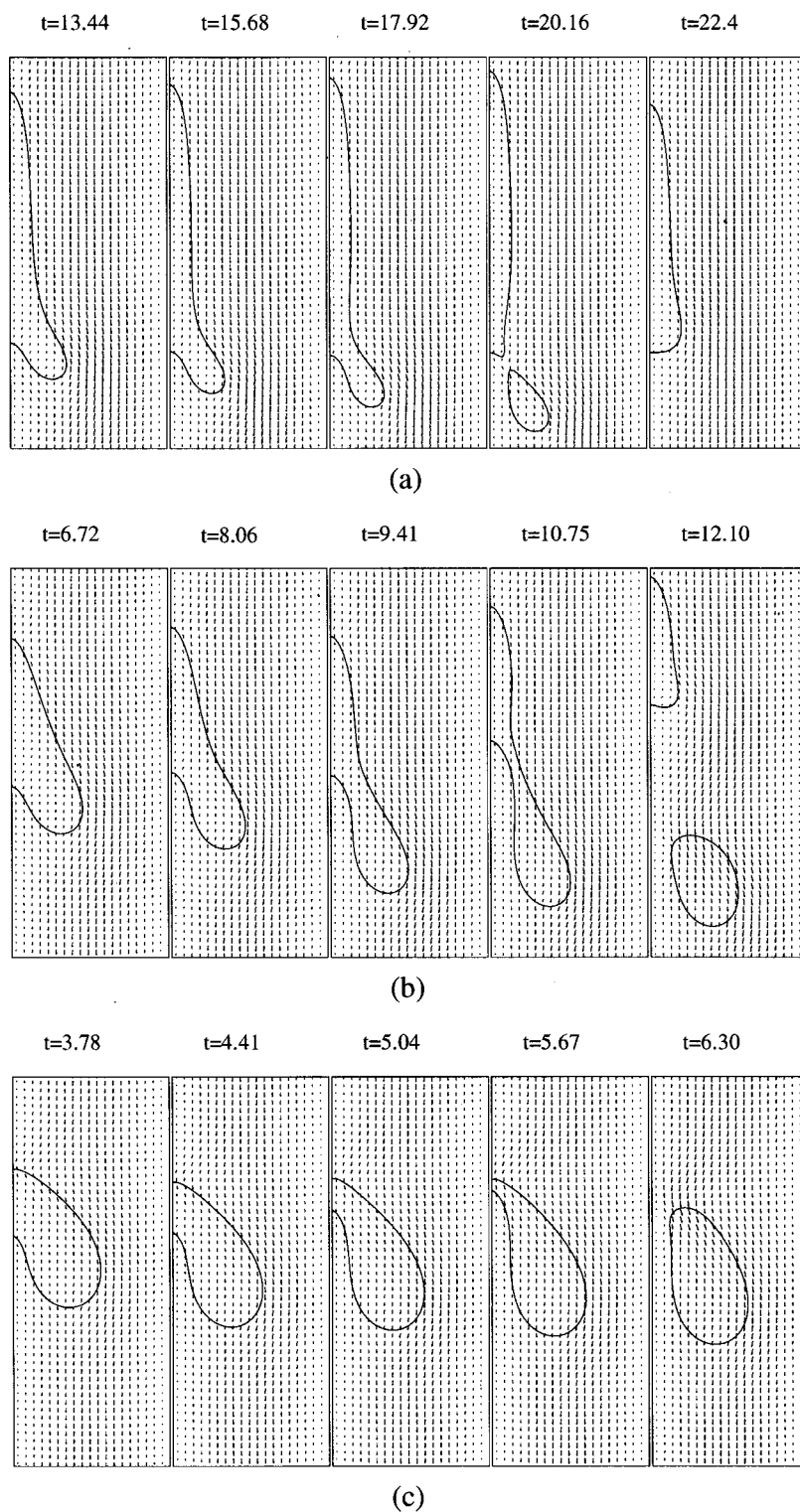
t=13.44   t=15.68   t=17.92   t=20.16   t=22.4

(a)

t=6.72   t=8.06   t=9.41   t=10.75   t=12.10

(b)

FIG. 7. Velocity fields near the droplet, corresponding to Fig. 6.

t=3.78   t=4.41   t=5.04   t=5.67   t=6.30

(c)

tact angle. It is clear that the critical Bond number decreases as the contact angle increases.

2. Effect of Bond number

Figure 10 illustrates the dependency of a steady-state value of the nondimensional wet length b/b_0 on the Bond number B_0, with a density ratio $\rho_2/\rho_1 = 1$, viscosity ratio $\nu_2/\nu_1 = 1$, droplet size $A/h^2 = 0.31$, and three contact angles ($\theta = 78°$, $90°$, and $118°$). Different Bond numbers are ob-

tained by changing g, the gravitational factor. At a low Bond number, b/b_0 decreases with the increase of B_0 in all cases. At $B_0 = 0.1843$, for the wetting case, b/b_0 reaches its minimum and begins to increase, while b/b_0 in the other cases keeps decreasing. As B_0 exceeds 0.2439 (the critical Bond number for the nonwetting droplet with $\theta = 118°$), the nonwetting droplet totally detaches from the wall (see Figs. 9 and 6 for details). When B_0 is about 0.2457, b/b_0 for the case of $\theta = 90°$ reaches its minimum and begins to increase.
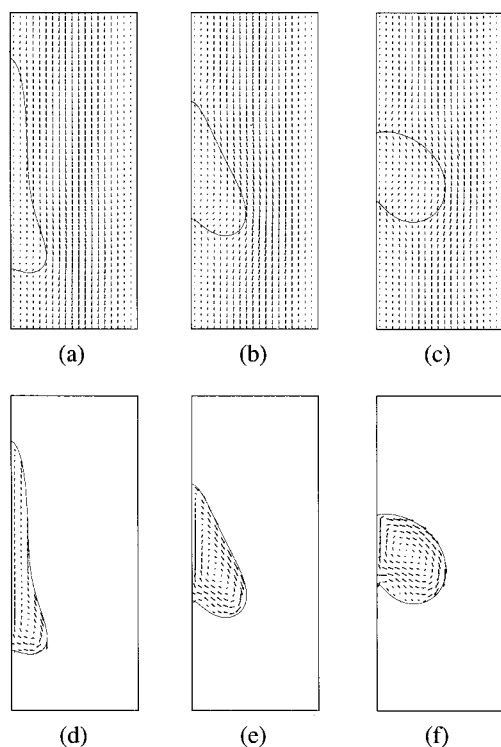
Phys. Fluids, Vol. 14, No. 9, September 2002

Displacement of a 2D immiscible droplet 3211

FIG. 8. Velocity fields near the steadily sliding droplet: (a) velocity profile near the droplet with static contact $\theta = 78°$ at $B_0 = 0.7985$, (b) velocity profile near the droplet with static contact $\theta = 90°$ at $B_0 = 0.5835$, (c) velocity profile near the droplet with static contact $\theta = 118°$ at $B_0 = 0.2150$, (d) velocity profile within the droplet for case (a) minus average droplet velocity, (e) velocity profile within the droplet for case (b) minus average droplet velocity, (f) velocity profile within the droplet for case (c) minus average droplet velocity.

Figure 11 shows the dependency of the steady-state value of the dimensionless contact-line velocity $\mu V_{cl}/\sigma$ (or the droplet velocity, since the shape of the droplet does not change with time any more) on the Bond number. For $\theta = 90°$ or $\theta = 118°$, this velocity is linear in B_0, meaning that

FIG. 10. Dependency of the steady-state wet length between the droplet and the wall on the Bond number. Other parameters are the same as in Fig. 2.

the droplet translates more rapidly as B_0 increases. The slope for $\theta = 90°$ is smaller than that for $\theta = 118°$. For the wetting case, however, there are two regions where the contact-line velocity varies linearly. The transition between these regions is $0.4300 \leq B_0 \leq 0.6142$, which corresponds to the region where b/b_0 increases rapidly, as seen in Fig. 10, and thus corresponds to the region where the droplet shape changes significantly, as seen in Fig. 12(a). Figure 12 shows the steady-state shape of the droplet at different Bond numbers.

3. Effect of droplet size

Figure 13 shows the dependency of the critical Bond number on the dimensionless area A/h^2 of the droplet, at $\theta = 78°$, 90°, and 118°. The density and viscosity ratios be-

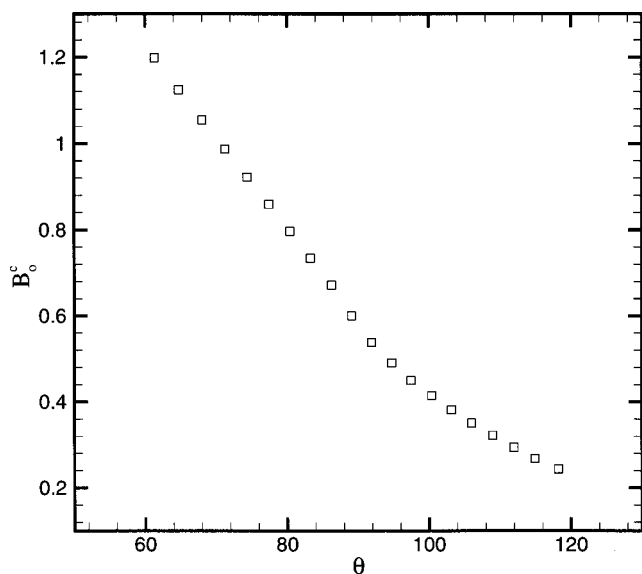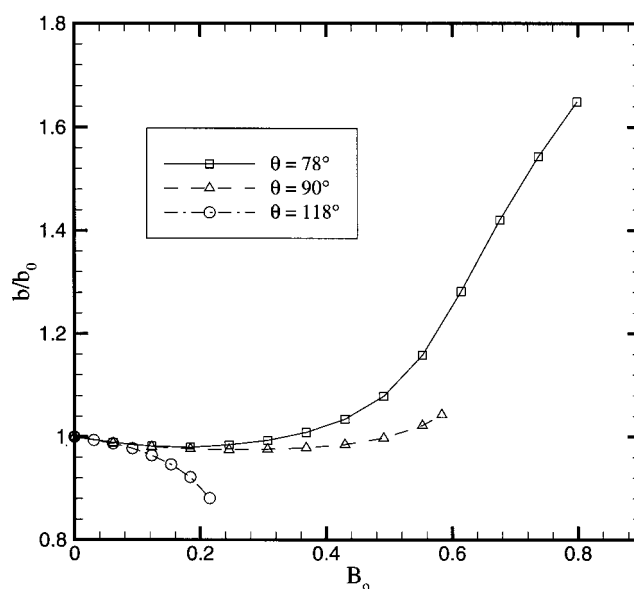

FIG. 9. Dependency of the critical Bond number (B_0^c) on the contact angle (θ). Other parameters are the same as in Fig. 2.
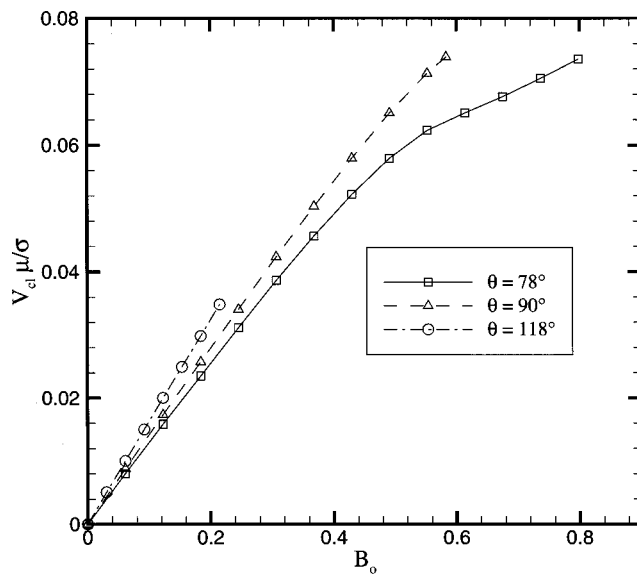

FIG. 11. Dependency of the steady-state contact-line velocity on the Bond number. Other parameters are the same as in Fig. 10.
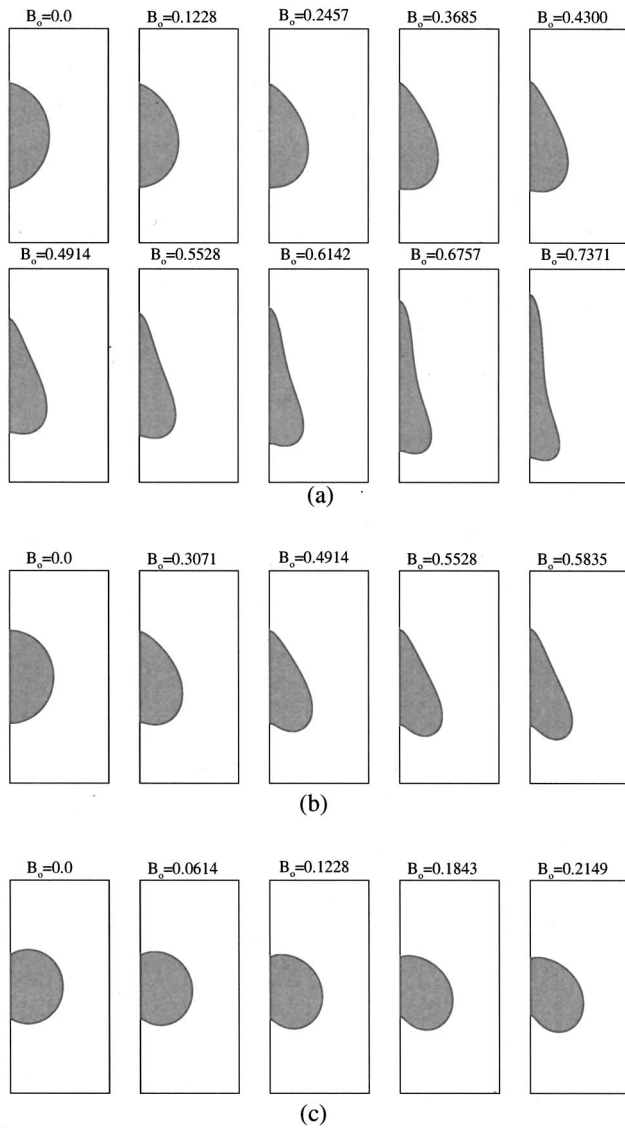
FIG. 12. The steady-state shape of the droplet at different Bond numbers. Other parameters are the same as in Fig. 2: (a) $\theta=78°$, (b) $\theta=90°$, (c) $\theta=118°$.

FIG. 13. The dependency of the critical Bond number on the dimensionless area of the static droplet, with $\rho_2/\rho_1=1$, $\nu_2/\nu_1=1$, $g_{12}=g_{21}=0.2$, and contact angles $\theta=78°$, $\theta=90°$, and $\theta=118°$.

cous forces between them. As a result, all or part of the droplet is able to detach from the wall or pinch off from the rest of it at a smaller body force strength.

4. Effects of density and viscosity ratios

We also performed the simulations of other cases with various density and viscosity ratios. The results are summarized in Table II. The dimensionless droplet area is 0.31. Increasing the viscosity of the droplet increases the viscous forces between the droplet and the displacing fluid, and hence decreases the critical Bond number. Increasing the density of the droplet, however, results in a higher critical Bond number. The reason is understandable: Displacement

tween the droplet and the displacing fluid are both 1. As the area of the droplet increases, the critical Bond number increases monotonically. It is helpful to study the effect of A on the critical capillary number, which is the ratio of viscous to surface forces and defined as $C_a=U\mu_1/\sigma$ by Schleizer and Bonnecaze.[19] Noticing here that $\rho_1=\rho_2$ and $\mu_1=\mu_2$, we have $C_a=U\mu_1/\sigma=\rho_2gh^2/\sigma$. The only difference between the definition of C_a and B_0 is that h^2, the square of the width of the channel, is used in the definition of C_a, while A, the area of the static droplet, is used in the definition of B_0. Figure 14 shows the dependency of the critical capillary number on the dimensionless area of the droplet. It is clear that the critical capillary number decreases monotonically as the static droplet area increases, which is intuitively correct and confirms the conclusion of Schleizer and Bonnecaze. As the droplet area increases, the relative velocity between the droplet and the displacing fluid increases and so do the vis-
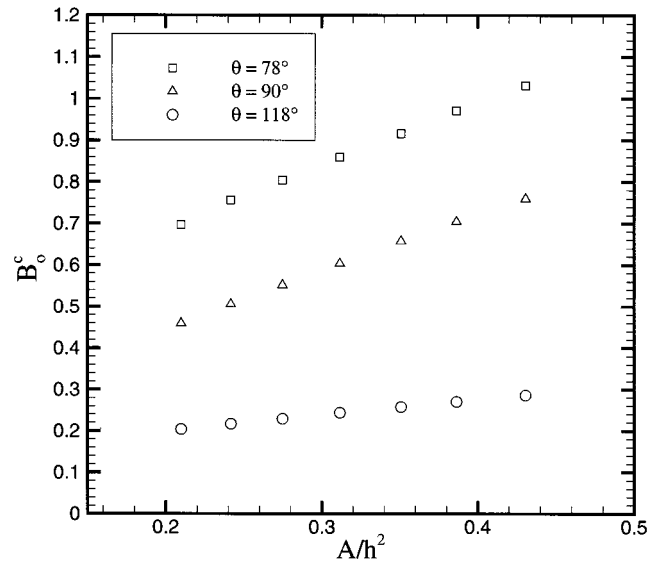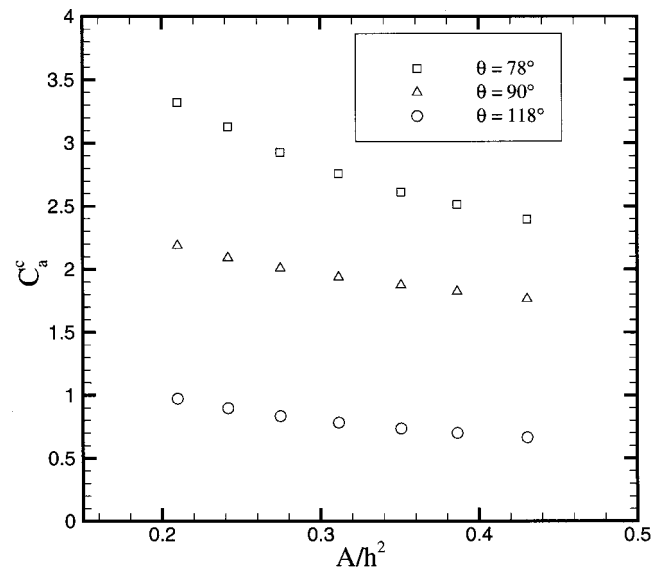

FIG. 14. The dependency of the critical capillary number on the dimensionless area of the static droplet, with $\rho_2/\rho_1=1$, $\nu_2/\nu_1=1$, $g_{12}=g_{21}=0.2$, and contact angles $\theta=78°$, $\theta=90°$, and $\theta=118°$.

Phys. Fluids, Vol. 14, No. 9, September 2002

Displacement of a 2D immiscible droplet   3213

TABLE II. Effect of viscosity and density ratios on the critical Bond number.

θ (deg)	ν_2/ν_1	ρ_2/ρ_1	B_0^c
78	1	1	0.8593
78	0.5	1	0.9847
78	2	1	0.5389
78	1	2	1.3527
78	1	0.5	0.4679
90	1	1	0.6037
90	0.5	1	0.7205
90	2	1	0.4364
90	1	2	1.0217
90	1	0.5	0.3849
118	1	1	0.2439
118	0.5	1	0.3095
118	2	1	0.2127
118	1	2	0.4009
118	1	0.5	0.1993

of a heavy fluid by a light one is more difficult than otherwise, provided other conditions are the same.

IV. CONCLUSIONS

We have simulated the displacement of a two-dimensional immiscible droplet of various wettabilities in a channel, subject to gravitational forces by the LB method. We found that at a very small Bond number, the droplet with different contact angles behaved similarly, the wet length between the droplet and the wall decreased with time until a steady shape was reached, which was different from the numerical results of Schleizer and Bonnecaze.[19] Their simulations showed that the wetting droplet spread along the wall at any capillary number. One possible reason of the discrepancy might be due to the presence of contact angle hysteresis in our simulations, since we made no assumption about the relationship between the contact angle and the velocity of the contact line. Hence, the advancing and receding contact angles were different from the static one in our study. As indicated in their paper, including the effects of contact angle hysteresis might significantly change the results. Our simulation results showed that these effects were more important at very small Bond number because when the droplet slid very slowly, the contact line yielded first would have a more pronounced effect on the behavior of the droplet.

As the Bond number increased, we found that the time evolution curves of the dimensionless wet length at different contact angles separated from each other. There also existed a critical Bond number, above which no steadily sliding droplet would be observed and the entire droplet would detach from the wall, or the upper portion of the droplet would pinch off from the lower portion of it, depending on its static contact angle. Increasing the contact angle resulted in a larger fraction of droplet being entrained in the bulk. Our observations are in line with the simulation results and the assertion by Schleizer and Bonnecaze.[19] We also found as a general trend that the critical Bond number decreased as the contact angle increased.

In the nonwetting droplet displacement, the steady-state wet length decreased monotonically and the steady-state velocity of the contact lines increased linearly as the Bond number increased. For the case of a contact angle less than or equal to 90°, the situation was more complicated. The steady-state wet length decreased first and then increased as the Bond number increased. When $\theta = 90°$, the steady-state velocity of the contact lines also increased linearly with the increase of the Bond number but with a smaller slope than when $\theta = 118°$. When $\theta = 78°$, however, the steady-state contact-line velocity varied linearly in two regions. The transition between the two regions corresponded to the region where there was a great change in the droplet shape.

We also performed simulations with various droplet sizes, density ratios, and viscosity ratios and found that with the increase of the viscosity ratio, or with the decrease of the density ratio, the critical Bond number decreased; with the increase of the droplet size, the critical Bond number increased, and the critical capillary number decreased.

The LB method used here is not limited to simulating the displacement of an immiscible droplet in a channel with flat, solid boundaries. It may also be effective in simulating the displacement of partially miscible fluids in complex geometries, which is the topic of our future work.

[1] R. G. Cox, "The dynamics of the spreading of liquids on a solid surface," J. Fluid Mech. **168**, 169 (1986).

[2] H. Zhou and C. Pozrikidis, "Pressure-driven flow of suspensions of liquid drops," Phys. Fluids **6**, 80 (1994).

[3] A. Borhan and C. F. Mao, "Effect of surfactants on the motion of drops through circular tubes," Phys. Fluids A **4**, 2628 (1992).

[4] T. M. Tsai and M. J. Miksis, "Dynamics of a drop in a constricted capillary tube," J. Fluid Mech. **274**, 197 (1994).

[5] E. B. Dussan, "On the ability of drops to stick to surfaces of solids," J. Fluid Mech. **174**, 381 (1987).

[6] X. Li and C. Pozrikidis, "Shear flow over a liquid drop adhering to a solid surface," J. Fluid Mech. **307**, 167 (1996).

[7] J. Q. Feng and O. A. Basaran, "Shear flow over a translationally cylindrical bubble pinned on a slot in a plane wall," J. Fluid Mech. **275**, 351 (1994).

[8] P. Dimitrakopoulos and J. J. L. Higdon, "Displacement of fluid droplets from solid surfaces in low-Reynolds-number shear flows," J. Fluid Mech. **336**, 351 (1997).

[9] P. Dimitrakopoulos and J. J. L. Higdon, "On the displacement of three-dimensional fluid droplets adhering to a plane wall in viscous pressure-driven flows," J. Fluid Mech. **435**, 327 (2001).

[10] E. B. Dussan, "The moving contact line: the slip boundary condition," J. Fluid Mech. **77**, 665 (1976).

[11] L. M. Hocking, "A moving fluid interface on a rough surface," J. Fluid Mech. **76**, 801 (1976).

[12] K. M. Jansons, "Moving contact lines on a two-dimensional rough surface," J. Fluid Mech. **154**, 1 (1985).

[13] M. Y. Zhou and P. Sheng, "Dynamics of immiscible fluid displacement in a capillary tube," Phys. Rev. Lett. **64**, 882 (1990).

[14] J. Koplik, J. R. Banavar, and J. F. Willemsen, "Molecular dynamics of a Poiseuille flow and moving contact lines," Phys. Rev. Lett. **60**, 1282 (1988).

[15] Y. D. Shikhmurzaev, "Moving contact lines in liquid/liquid/solid systems," J. Fluid Mech. **334**, 211 (1997).

[16] L. Fan, H. Fang, and Z. Lin, "Simulation of contact line dynamics in a

two-dimensional capillary tube by the lattice Boltzmann model," Phys. Rev. E **63**, 051603 (2001).

[17] P. Raiskinmaki, A. Koponen, J. Merikoski, and J. Timonen, "Spreading dynamics of three-dimensional droplets by the lattice-Boltzmann method," Comput. Mater. Sci. **18**, 7 (2000).

[18] D. Grubert and J. M. Yeomans, "Mesoscale modeling of contact line dynamics," Comput. Phys. Commun. **121–122**, 236 (1999).

[19] A. D. Schleizer and R. T. Bonnecaze, "Displacement of a two-dimensional immiscible droplet adhering to a wall in shear and pressure-driven flows," J. Fluid Mech. **383**, 29 (1998).

[20] F. J. Alexander, S. Chen, and D. W. Grunau, "Hydrodynamics spinodal decomposition: Growth kinetics and scaling," Phys. Rev. B **48**, 634 (1993).

[21] M. Cieplak, "Rupture and coalescence in 2-dimensional cellular-automata fluids," Phys. Rev. E **51**, 4353 (1995).

[22] S. Chen and G. D. Doolen, "Lattice Boltzmann method for fluid flows," Annu. Rev. Fluid Mech. **30**, 329 (1998).

[23] R. Benzi, S. Succi, and M. Vergassola, "The lattice Boltzmann-equation—Theory and applications," Phys. Rep. **222**, 145 (1992).

[24] D. H. Rothman and S. Zaleski, "Lattice-gas models of phase separation: Interfaces, phase transitions and multiphase flow," Rev. Mod. Phys. **66**, 1417 (1994).

[25] S. Chen, S. P. Dawson, G. D. Goolen, D. R. Janecky, and A. Lawniczak, "Lattice methods and their applications to reacting systems," Comput. Chem. Eng. **19**, 617 (1995).

[26] Y. Qian, S. Succi, and S. A. Orszag, "Recent advances in lattice Boltzmann computing," Annu. Rev. Comput. Phys. **3**, 195 (1995).

[27] D. Zhang, R. Zhang, S. Chen, and W. E. Soll, "Pore scale study of flow in porous media: Scale dependency, REV, and statistical REV," Geophys. Res. Lett. **27**, 1195 (2000).

[28] Q. Kang, D. Zhang, S. Chen, and X. He, "Lattice Boltzmann simulation of chemical dissolution in porous media," Phys. Rev. E **65**, 036318 (2002).

[29] A. K. Gunstensen, D. H. Rothman, S. Zaleski, and G. Zanetti, "Lattice Boltzmann model of immiscible fluids," Phys. Rev. A **43**, 4320 (1991).

[30] D. Grunau, S. Chen, and K. Eggert, "A lattice Boltzmann model for multiphase fluid flows," Phys. Fluids A **5**, 2557 (1993).

[31] X. Shan and H. Chen, "Lattice Boltzmann model for simulation flows with multiple phases and components," Phys. Rev. E **47**, 1815 (1993).

[32] X. Shan and H. Chen, "Simulation of nonideal gases and liquid-gas phase transitions by the lattice Boltzmann equation," Phys. Rev. E **49**, 2941 (1994).

[33] X. Shan and G. D. Doolen, "Diffusion in a multicomponent lattice Boltzmann equation model," Phys. Rev. E **54**, 3614 (1996).

[34] X. Shan and G. D. Doolen, "Multicomponent lattice-Boltzmann model with interparticle interaction," J. Stat. Phys. **81**, 379 (1995).

[35] S. Hou, X. Shan, Q. Zou, G. Doolen, and W. Soll, "Evaluation of two lattice Boltzmann models for multiphase flows," J. Comput. Phys. **138**, 695 (1997).

[36] M. Swift, W. Osborn, and J. Yeomans, "Lattice Boltzmann simulation of nonideal fluids," Phys. Rev. Lett. **75**, 830 (1995).

[37] M. Swift, S. Orlandini, W. Osborn, and J. Yeomans, "Lattice Boltzmann simulations of liquid-gas and binary-fluid systems," Phys. Rev. E **54**, 5041 (1996).

[38] R. Zhang, "Lattice Boltzmann approach for immiscible multiphase flow," Ph.D. thesis, Department of Mechanical Engineering, University of Delaware, 1999.

[39] X. He, S. Chen, and R. Zhang, "A lattice Boltzmann scheme for incompressible multiphase flow and its application in simulation of Rayleigh–Taylor instability," J. Comput. Phys. **152**, 642 (1999).

[40] A. K. Gunstensen and D. H. Rothman, "Lattice-Boltzmann studies of immiscible two-phase flow through porous media," J. Geophys. Res. **98**, 6431 (1993).

[41] S. Chen, G. D. Doolen, and K. G. Eggert, "Lattice-Boltzmann fluid dynamics—A versatile tool for multiphase fluid dynamics and other complicated flows," Los Alamos Sci. **22**, 98 (1994).

[42] N. S. Martys and H. Chen, "Simulation of multicomponent fluids in complex three-dimensional geometries by the lattice Boltzmann method," Phys. Rev. E **53**, 743 (1996).

[43] K. Langaas and D. Grubert, "Lattice Boltzmann simulations of wetting and its application to disproportionate permeability reducing gel," J. Pet. Sci. Eng. **24**, 199 (1999).

[44] X. He, R. Zhang, S. Chen, and G. D. Doolen, "On three-dimensional Rayleigh–Taylor instability," Phys. Fluids **11**, 1143 (1999).

[45] H. Chen, S. Chen, and W. H. Matthaeus, "Recovery of the Navier–Stokes equations using a lattice-gas Boltzmann method," Phys. Rev. A **45**, R5339 (1992).

[46] S. Hou, "Lattice Boltzmann method for incompressible, viscous flow," Ph.D. thesis, Department of Mechanical Engineering, Kansas State University, 1995.

[47] B. R. Sehgal, R. R. Nourgaliev, and T. N. Dinh, "Numerical simulation of droplet deformation and break-up by lattice Boltzmann method," Prog. Nucl. Energy **34**, 471 (1999).

[48] F. A. L. Dullien, *Porous Media: Fluid Transport and Pore Structure* (Academic, New York, 1992).

[49] S. Wolfram, "Cellular automaton fluids. 1: Basic theory," J. Stat. Phys. **45**, 471 (1986).

[50] P. Lavallee, J. P. Boon, and A. Noullez, "Boundaries in lattice gas flows," Physica D **47**, 233 (1991).

[51] Z. L. Yang, T. N. Dinh, R. R. Nourgaliev, and B. R. Sehgal, "Numerical investigation of bubble growth and detachment by the lattice-Boltzmann method," Int. J. Heat Mass Transf. **44**, 195 (2001).